Supporting Information

Functional-Oriented Design of Gradient Composite Fluoride Interphase for Enhanced Silicon Anode Performance

Yu Jing[a], *Zhixing Wang*[a, b, c], *Huajun Guo*[a, b, c], *Xinhai Li*[a, b, c], *Hui Duan*[a, b, c], *Wenjie Peng*[a, b, c], *Guochun Yan*[a, b, c], *Guangchao Li*[a, b, c*], *Jiexi Wang*[a, b, c]

[a] School of Metallurgy and Environment, Central South University, 410083 Changsha, China

[b] Engineering Research Center of the Ministry of Education for Advanced Battery Materials, Central South University, Changsha, 410083, China

[c] Hunan Provincial Key Laboratory of Nonferrous Value-Added Metallurgy, Central South University, Changsha, 410083, China

Corresponding author e-mail address: guangchao_li@csu.edu.cn;

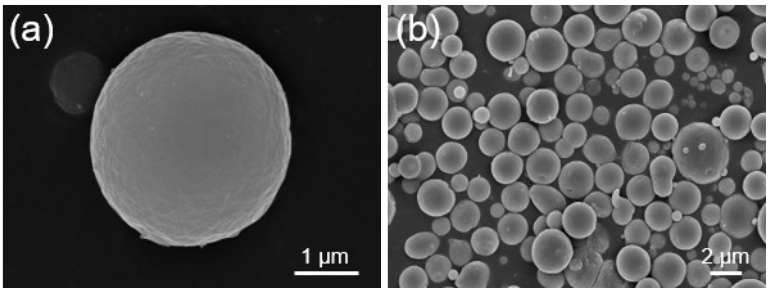

Figure S1. (a, b) SEM images of pristine $AlSi_{12}$ alloy

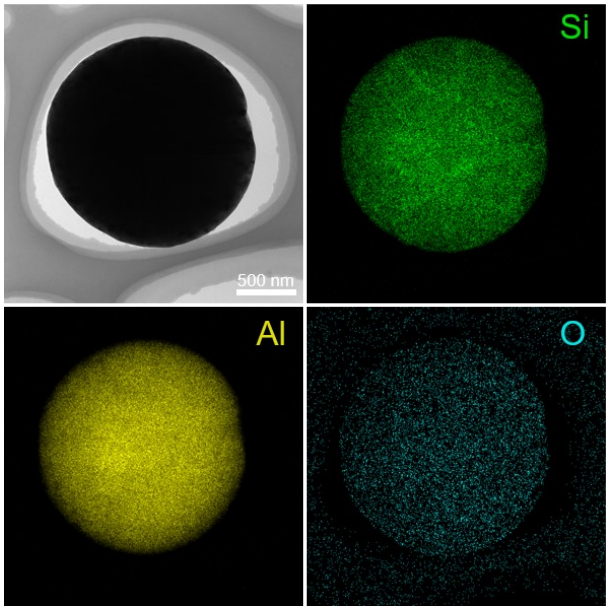

Figure S2. TEM and elemental mapping images of $AlSi_{12}$ alloy

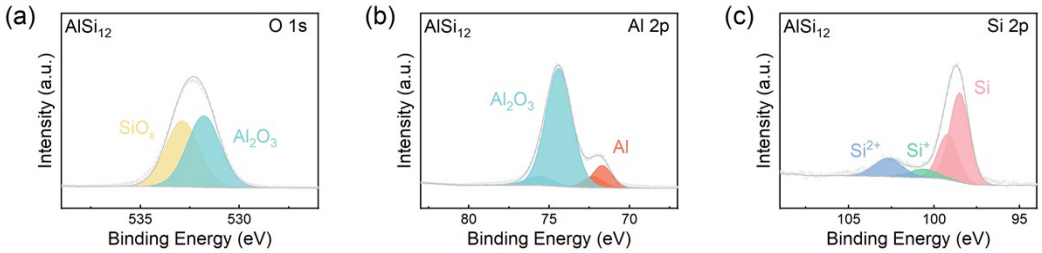

Figure S3. The XPS spectra of $AlSi_{12}$ alloy. (a) O 1s, (b) Al 2p, (c) Si 2p

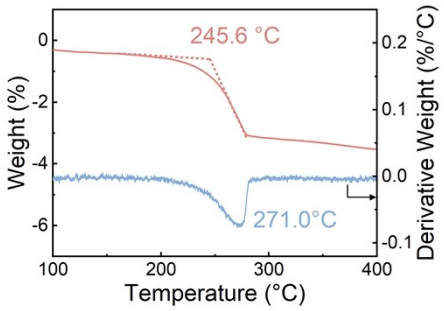

Figure S4 DTG curves of LSAF-1

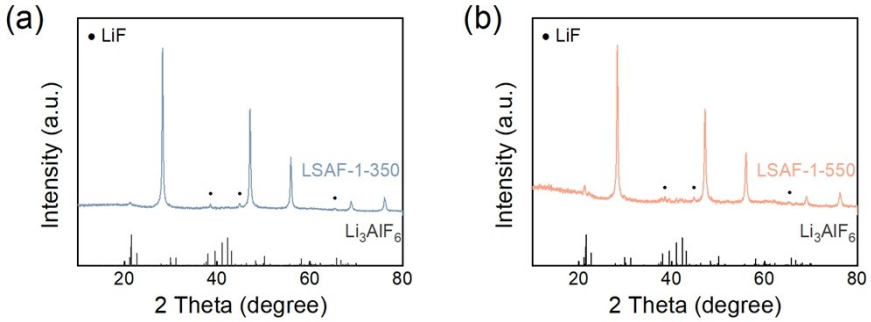

Figure S5. XRD pattern of LSAF-1 after heat treatment at (a) 350 and (b) 550 °C

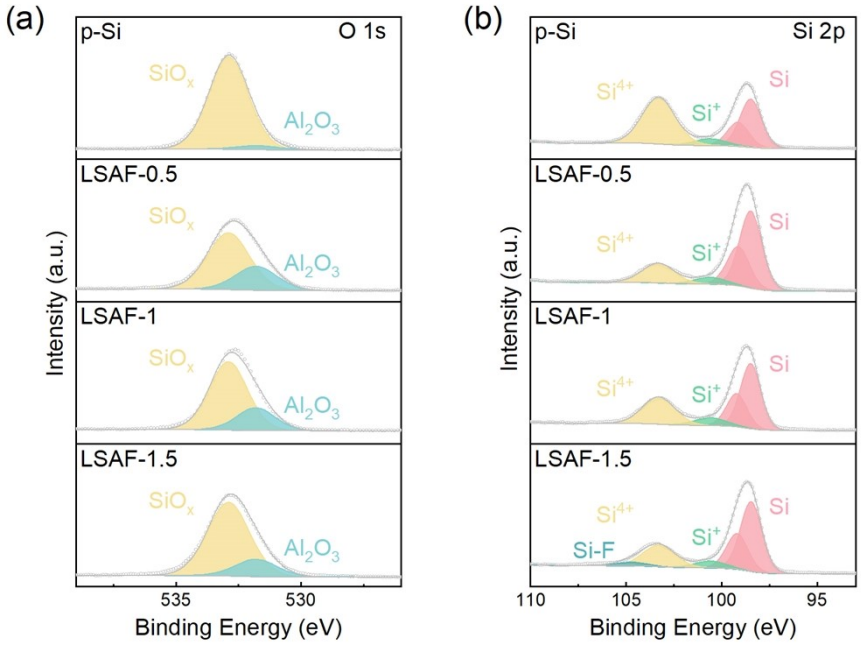

Figure S6. (a) O 1s and (b) Si 2p XPS spectra of materials

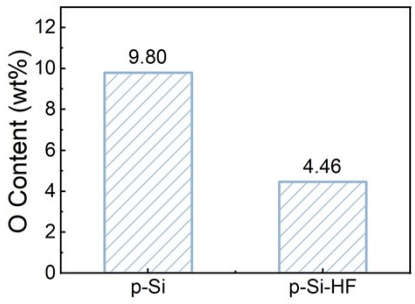

Figure S7. Comparison of the oxygen content in p-Si before and after HF etching

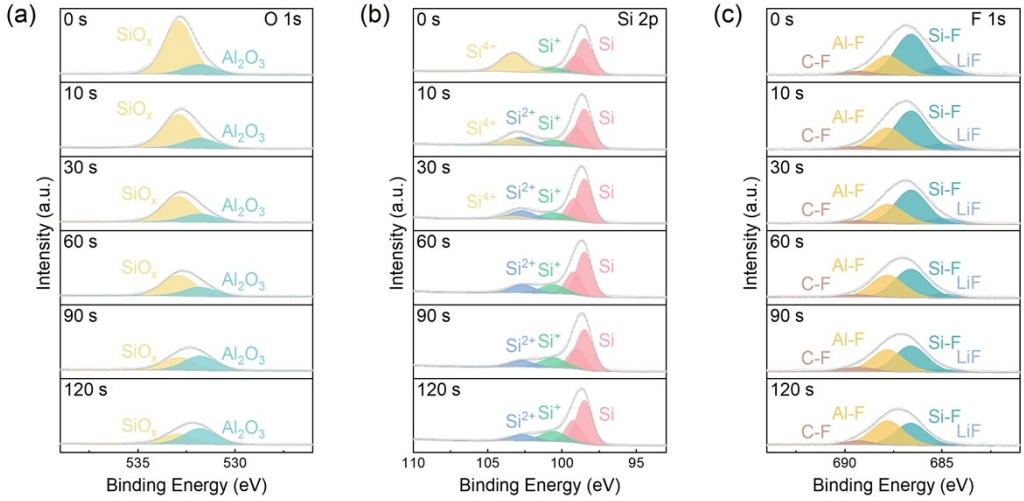

Figure S8. (a) O 1s, (b) Si 2p and (c) F 1s spectra of LSAF-1 after different Ar^+ etching times

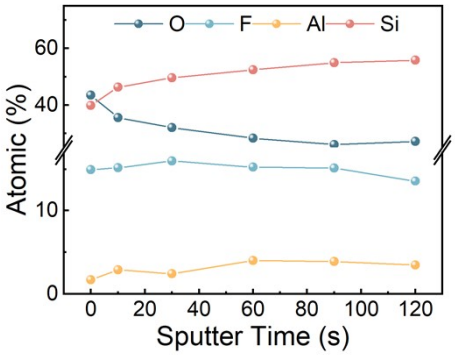

Figure S9. The atomic percentage of each element in the LSAF-1 sample with sputter time

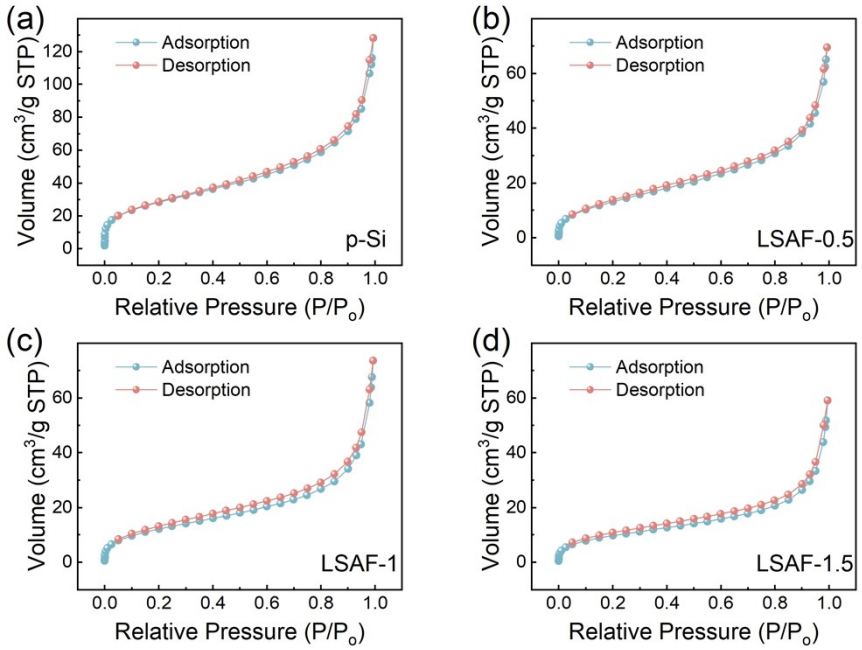

Figure S10. N_2 isothermal adsorption/desorption curves of (a) p-Si, (b) LSAF-0.5, (c) LSAF-1, (d) LSAF-1.5

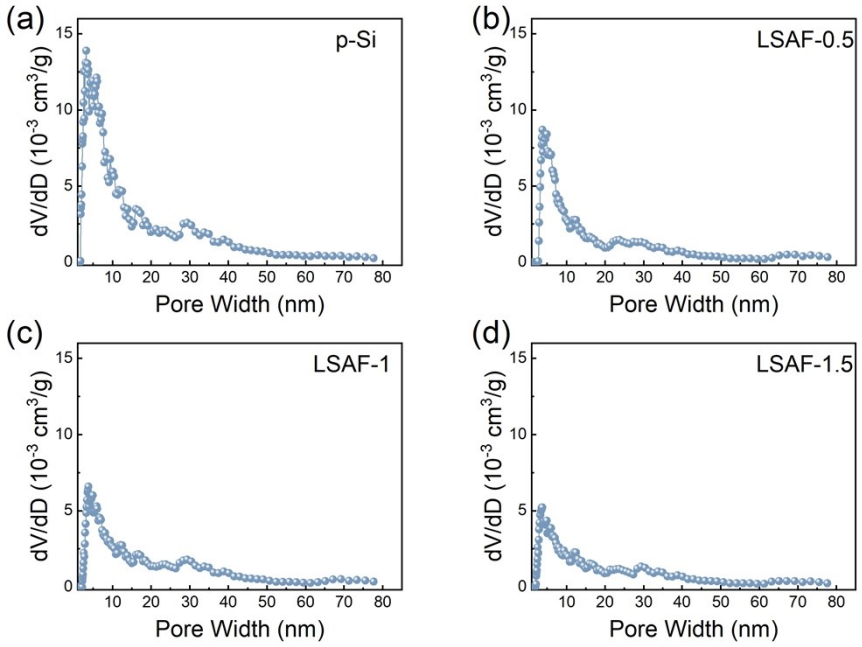

Figure S11. Pore size distribution of (a) p-Si, (b) LSAF-0.5, (c) LSAF-1, (d) LSAF-1.5

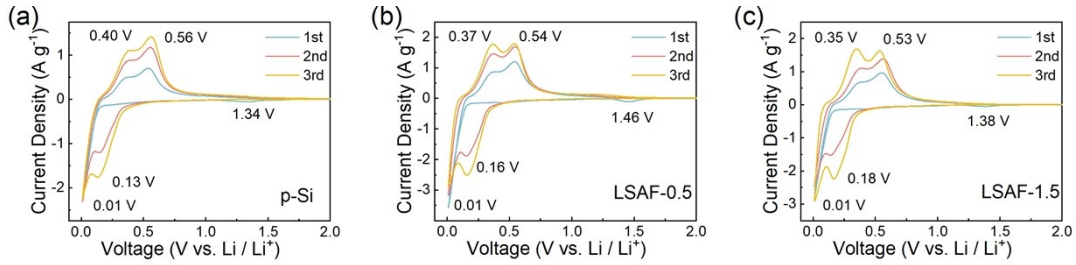

Figure S12. CV curves of (a) p-Si, (b) LSAF-0.5, (c) LSAF-1.5

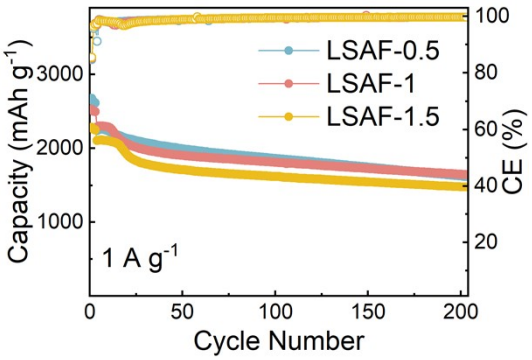

Figure S13. Cycle performance of materials with different coating contents at 1 A g^{-1}

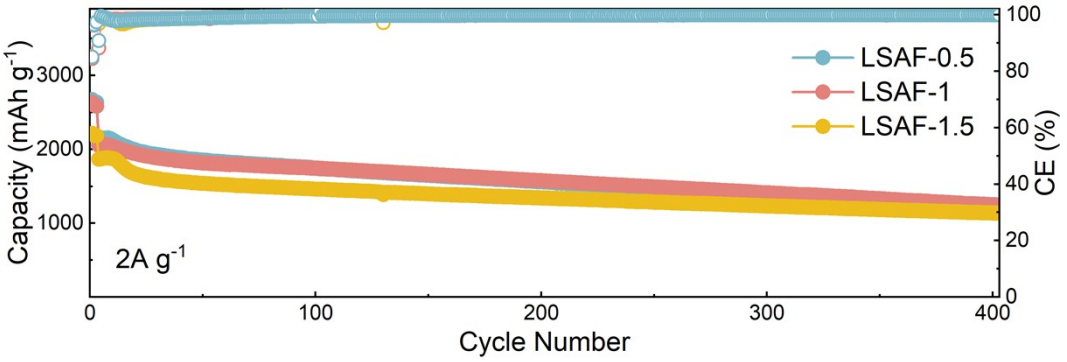

Figure S14. Cycle performance of materials with different coating contents at 2 A g^{-1}

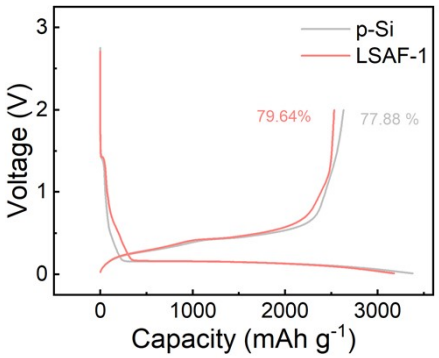

Figure S15. charge-discharge curves under 45 ℃

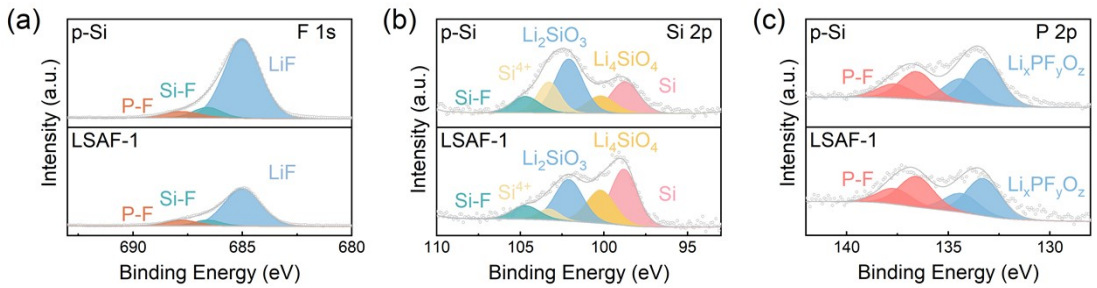

Figure S16. (a) F 1s, (c) Si 2p and (d) P 2p XPS spectra of electrodes after 3 cycles at 0.2 A g^{-1}

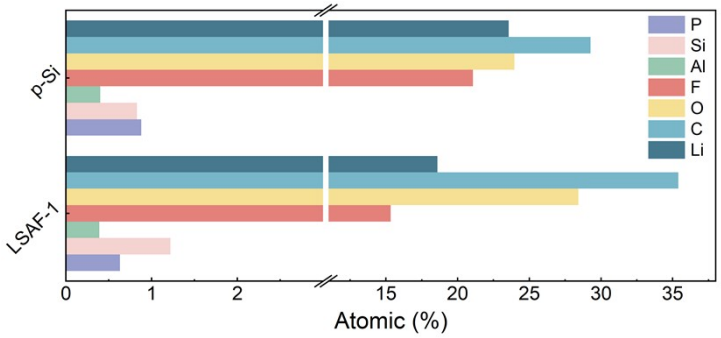

Figure S17. The atomic percentage of each element in the SEI film

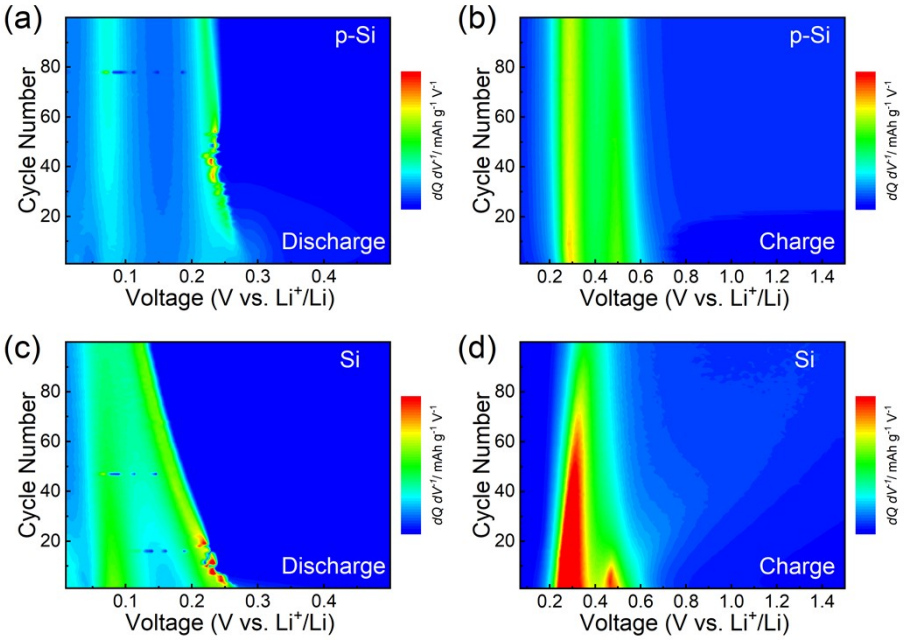

Figure S18. dQ/dV mappings for the (a) discharging and (b) charging processes of p-Si. dQ/dV mappings for the (c) discharging and (d) charging processes of Si

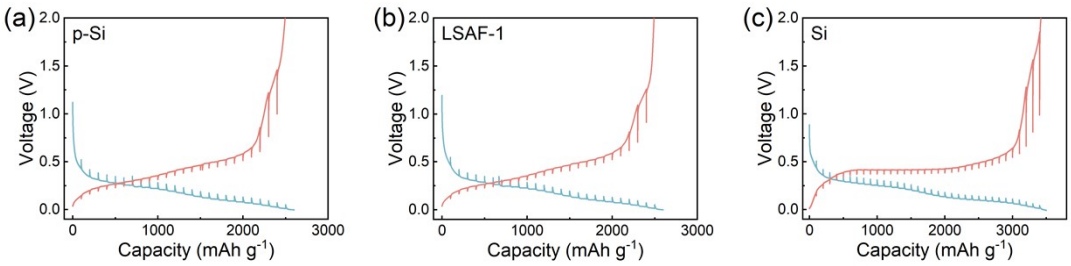

Figure S19. GITT curves of (a) p-Si, (b) LSAF-1, (c) Si

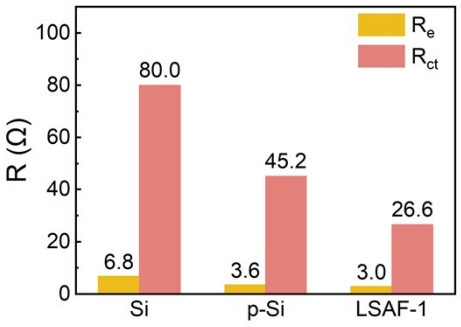

Figure S20. EIS fitting parameters of electrodes before cycling

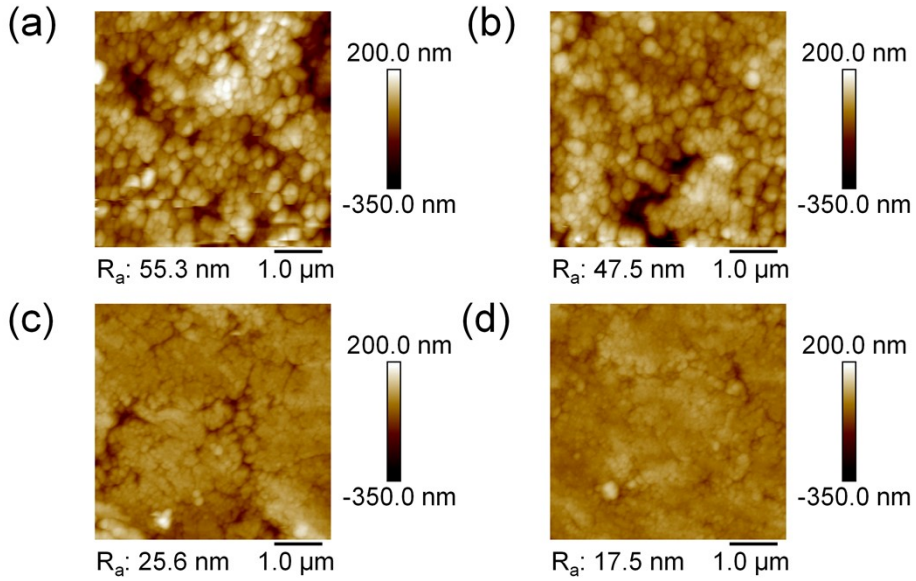

Figure S21. Surface roughness of electrodes in different regions. (a-b) p-Si; (c-d) LSAF-1.

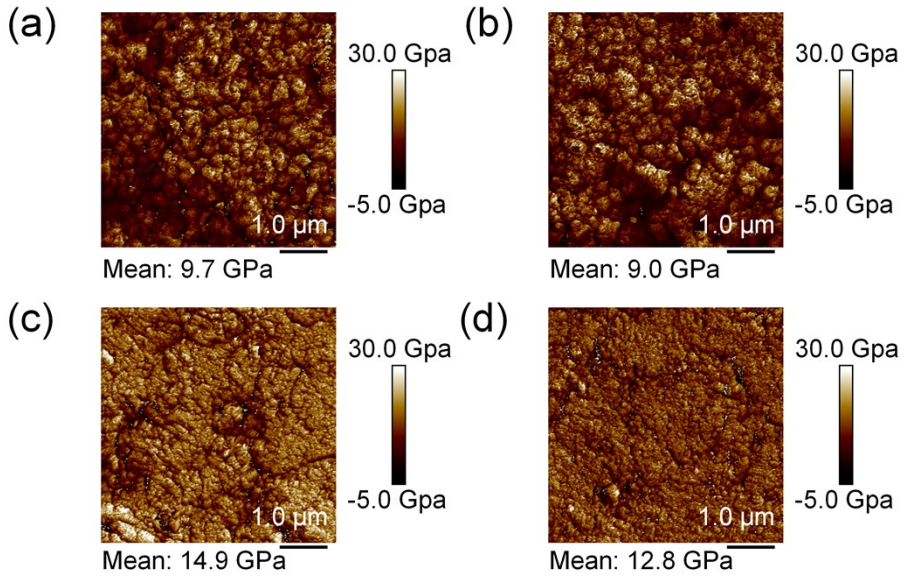

Figure S22. 2D plots of DMT modulus of electrodes in different regions. (a-b) p-Si; (c-d) LSAF-1.

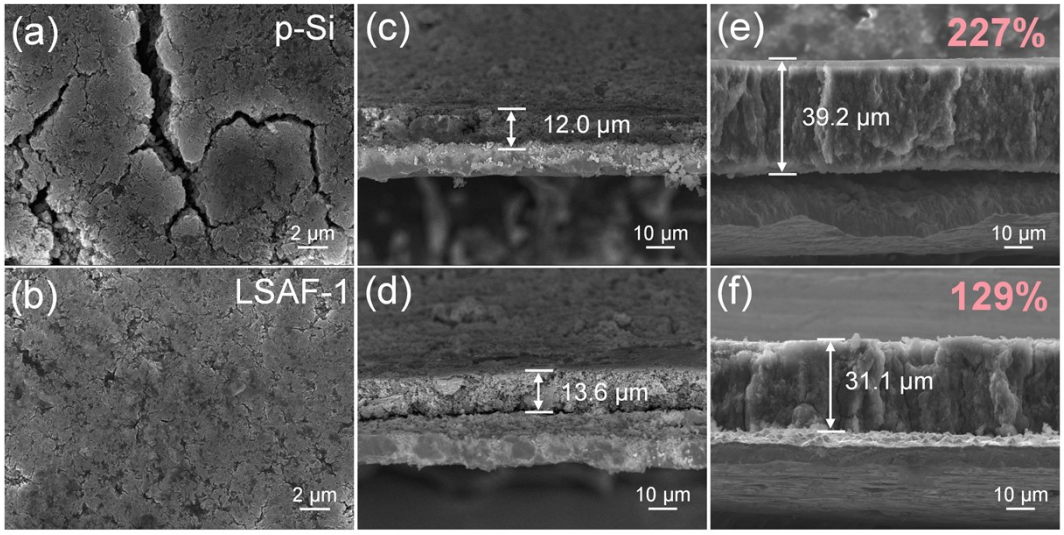

Figure S23. SEM images of p-Si and LSAF-1 anodes. (a-b) Top view after cycling; the cross-section view (c-d) before and (e-f) after cycling.

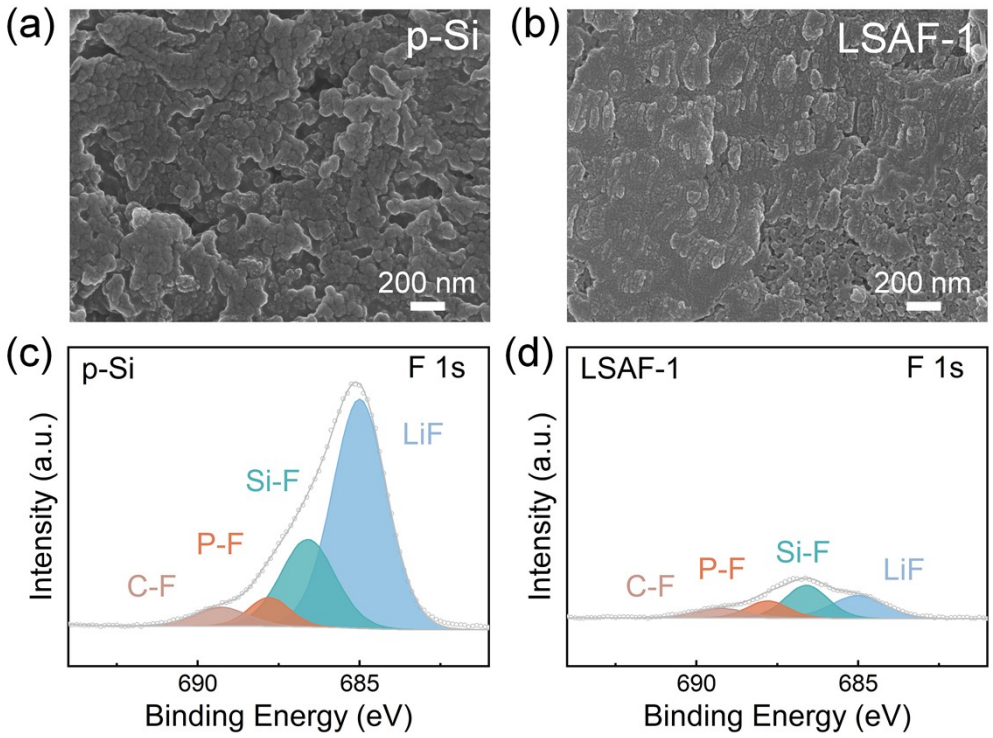

Figure S24. Surface morphology and chemical state analysis of electrodes after high-temperature cycling. SEM images of (a) p-Si and (b) LSAF-1 anodes. F 1s XPS spectra of (c) p-Si and (d) LSAF-1 anodes.

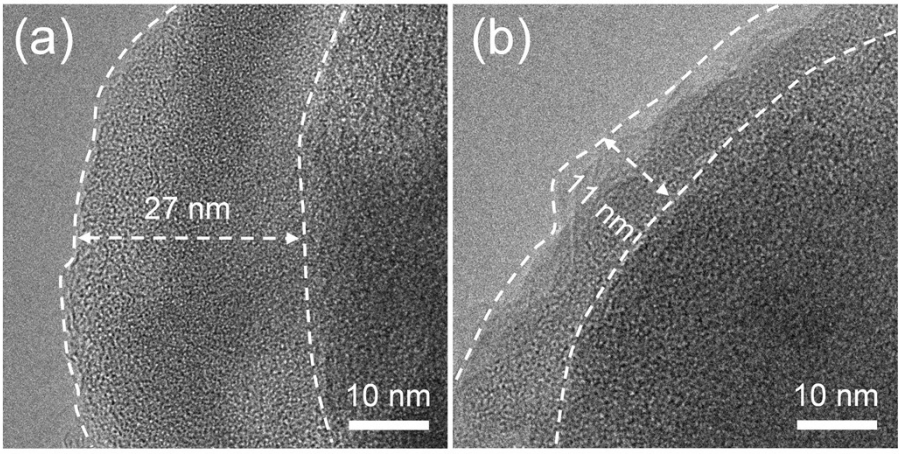

Figure S25. HRTEM images of (a) p-Si and (b) LSAF-1 anodes after cycling.